Composites Part B 234 (2022) 109686

Contents lists available at ScienceDirect

Composites Part B

journal homepage: www.elsevier.com/locate/compositesb

Effects of filler composition, loading, and geometry on the dielectric loss, partial discharge, and dielectric strength of liquid metal polymer composites

Robert E. Calabrese [a], Elizabeth Bury [b], Farhina Haque [a], Amanda Koh [b,**], Chanyeop Park [a,*]

[a] 406 Hardy Rd., 216 Simrall Hall, Mississippi State, MS, 39762, USA
[b] 3043 H.M. Comer, 245 7th Avenue, Tuscaloosa, AL, 35487, USA

ARTICLE INFO

Keywords:
Liquid metal
Dielectric loss
Partial discharge
Dielectric strength

ABSTRACT

With the goal of enabling the design of liquid metal polymer composites (LMPCs) with desired electrical and mechanical properties while preventing premature dielectric aging and failure, the dielectric breakdown characteristics of LMPCs containing galinstan (GaInSn), barium titanate (BTO), iron (Fe), and mixtures thereof are investigated. The dielectric properties including dielectric loss (tan δ), partial discharge inception electric field (PDIE), and breakdown electric field (E_{bd}) are investigated. According to the study, LMPCs with a higher overall filler concentration tend to show higher tan δ, lower PDIE, and lower E_{bd}. The study also demonstrates that these dielectric properties vary by the type of filler even with an equally maintained filler concentration. This is due to the distinct filler conductivity, permittivity, and geometry that cause differences in the electric field distribution within the composites. To provide further insights into the observed experimental results, finite element analysis (FEA) models were developed and analyzed.

1. Introduction

Stretchable electronics is a vast field that has applications such as wearable devices [1], energy storage, actuation, and thermal management [2]. To fabricate a truly inherently stretchable electronic device, the individual components of the device must be capable of withstanding deformation and high mechanical strain, which is commonly achieved by utilizing soft and stretchable materials. Previous research using soft materials for stretchable electronics has demonstrated increased human-device compatibility and decreased mechanical mismatch [2–4]. While polymers are often used as the basis of stretchable electronics, particularly as supports and continuous matrices, deformable conductive and dielectric materials are necessary to increase the electrical performance of soft devices. Traditional rigid materials that are used in electronic devices such as metals and ceramics lead to mechanical failure or reduced electrical performance when used in a soft system [1,5,6]. Room-temperature gallium-based liquid metal, specifically galinstan (GaInSn), has been a recent focus as a deformable conductor owing to its high conductivity and low modulus [7–10]. While there has been extensive work utilizing liquid metal alone as a deformable conductor [11–13], research has taken advantage of composites of soft polymeric matrices and conductive liquid metal to create soft dielectric materials [14,15]. By dispersing liquid metal into polymers, dielectric materials that can be utilized in capacitors, dielectric elastomers, actuators, and pressure sensors are created [2,16,17].

High dielectric constants (*i.e.*, relative permittivity) have been achieved through dispersing high concentrations of liquid metal in polymeric matrices [17,18]. While this approach has been successful, it has also led to materials with low dielectric breakdown strength [14], which must be avoided to ensure the dielectric reliability and to prevent the accelerated aging of technologies relying on the deformable dielectric materials. High concentrations of liquid metal also result in composites that are expensive, further reducing the technological potential of the material. Previous work has investigated multi-material blends, particularly solid material dispersions, as a potential method of achieving composites with high relative permittivity through functionalization [19–21] and fabricated such composites for application in elastomer actuators [22]. While research has been conducted to create

* Corresponding author.
** Corresponding author.
E-mail addresses: rec397@msstate.edu (R.E. Calabrese), egbury@crimson.ua.edu (E. Bury), fh317@msstate.edu (F. Haque), askoh@eng.ua.edu (A. Koh), chanyeop.park@ece.msstate.edu (C. Park).

https://doi.org/10.1016/j.compositesb.2022.109686
Received 22 December 2021; Received in revised form 22 January 2022; Accepted 24 January 2022
Available online 29 January 2022

multi-material blends with rigid materials and liquid metals demonstrating the promise of these materials and their high permittivity and low modulus [23–29], little has been researched to fundamentally understand their dielectric aging and failure mechanisms under electrical stresses. While including rigid fillers with liquid metal in a polymer composite may result in high relative permittivity, it is known that increasing rigid filler concentration results in a more brittle and rigid medium [5,30]. As such, it is necessary to understand the relationship between composite formulation and electrical properties to ensure that the deformable materials show high permittivity, low dielectric loss (tan δ), high partial discharge inception electric field (PDIE), and high breakdown electric field (E_{bd}) simultaneously.

The quality of dielectric materials, including those containing liquid metal ultimately depends on the electric field distribution within the materials. Depending on the conductivity and permittivity of the fillers used, the intensity of the internal electric field varies, leading to local hot spots of electric field concentrations. In general, high electric fields should be avoided as they energize electrons and cause ionization. Depending on the intensity of the electric field, the ionization process could either cause partial discharge (PD) or a dielectric breakdown. Unlike a dielectric breakdown, PD is a micro electric discharge that gradually erodes dielectric materials and reduces the remaining useful life of a device. On the other hand, dielectric breakdown indicates a destruction of an electrically insulating medium.

With the goal of improving the dielectric quality of liquid metal polymer composites (LMPCs) while achieving high relative permittivity and low cost, in this study, we replace portions of liquid metal with materials possessing relatively high conductivity and high permittivity – iron (Fe) [31] and barium titanate ($BaTiO_3$ or BTO) [32]. Composites consisting of GaInSn, BTO, or Fe, alone as well as the mixtures there of are interrogated with respect to tan δ, PDIE, and E_{bd}. A testbed was designed and constructed to investigate the dielectric characteristics of the composites. The samples were subjected to increasing magnitudes of voltage to identify their PD characteristics and dielectric strength. The experimental results were validated by finite element analysis (FEA) models that qualitatively simulate the electric field distribution within the composite samples. The results of this study contribute to the body of knowledge required for enabling the tunability of these multi-material composites in terms of dielectric properties required for soft electronics and advanced energy storage technologies.

2. Experiment

2.1. Material description

Galinstan, purchased from Rotometals (San Leandro, CA), with a concentration of 68.5% Ga, 21.5% In, 10% Sn was used as received. Iron (Fe) and barium titanate ($BaTiO_3$, BTO) were purchased from Chemical Store Inc. (Clifton, NJ) and Sigma-Aldrich (St. Louis, MO), respectively, and used as received. Particles were characterized with scanning electron microscopy (SEM) and x-ray diffraction (XRD) to determine particle size, shape, and crystal structure. Iron particles were found to have an irregular shape with a cubic crystal structure. BTO particles were roughly spherical and found to have a cubic crystalline structure. SEM and XRD results of the particles can be found in Figs. S5–S6. Vinyl-terminated and tri-methyl terminated polydimethylsiloxane (PDMS, Gelest, Inc.- Morrisville, PA) with molecular weights of 62,700 g/mol (DMS-V41, $1{\bullet}10^4$cSt) and 1250 g/mol (DMS-T11, 10 cSt), respectively, were used as the continuous polymer matrix. Platinum–cyclovinylmethylsiloxane complex catalyst (800 ppm) and tetrakis (dimethylsiloxy) silane cross-linker were both purchased from Gelest, Inc.

2.2. LMPC fabrication

Using a 1:1 vol/vol blend of V41:T11, all composites had filler compositions of 0, 10, or 30 vol% of GaInSn and 10, 20, or 30 vol% of either rigid filler, BTO, or Fe. To form composites, all components of each respective formulation were mixed using a Caframo (Ontario, Canada) High Torque Overhead Stirrer at 1800 rpm for 2 h. Subsequently, the catalyst and crosslinker were added and mixed for an additional 30 s, after which the samples were poured into circular polytetrafluoroethylene (PTFE) molds and left to cure at 82 °C for 72 h. During the formation of the composites in both mixing and curing stages, no macroscopic phase separation or aggregation of filler was observed. In addition, all cured samples were free-standing and exhibited no signs of morphology change during the course of characterization.

2.3. Dielectric loss measurement

Dielectric loss (tan δ) was measured at frequencies from 500 Hz to 5 MHz using a Keysight (Santa Rosa, CA) E4990A Impedance Analyzer with the 16451B Dielectric Test Fixture. All LMPC samples were free-standing and characterized in the cured state with a thickness of 1 mm and 0.5 mm to ensure there was no error as it related to the relative sizes of the fillers to the cured LMPC. No change in dispersion morphology was observed over the time span of the experiments.

2.4. PDIE and e_{bd} measurement testbed

Partial discharge (PD) and dielectric strength were measured using a custom designed testbed shown in Fig. 1 (a). The testbed consists of a high voltage electrode and a small container to hold the sample. The container consists of a small piece of PVC pipe sealed to an aluminum ground plate using silicone caulk. A brass sphere was connected to the top of the electrode to prevent corona discharge from occurring. The container was filled with transformer oil to suppress surface discharge and surface flashover, and each sample was placed between the high voltage electrode and ground plate to ensure that all PD occurs within the LMPC samples. For both PD and dielectric strength measurements, the top electrode was connected to a high voltage amplifier, while a coupling capacitor was also connected in parallel to the testbed for measuring PD. The amplifier, which is controlled by the signal generator shown in Fig. 1, acts as a high voltage source that triggers PD or dielectric breakdown in the LMPC samples. The output of the amplifier is monitored using an oscilloscope to validate the waveform and the magnitude of the voltage applied. The amplifier was set to generate a 60 Hz sinusoidal voltage signal, which is also known as the power frequency.

2.5. PDIE and E_{bd} measurement procedure

PD measurements were performed using the testbed and equipment shown in Fig. 1. Each sample was placed in the testbed submerged in transformer oil, the electrode and the ground plate were firmly touching the sample, and voltage was slowly increased until PD signals appeared in the measurement system (see Fig. S3). The voltage at which PD starts to appear, which is known as the partial discharge inception voltage (PDIV), was recorded. This process was repeated three times for each sample. The three PDIV measurements were then averaged, and the value was divided by the thickness of the sample to derive the partial discharge inception electric field (PDIE).

Dielectric strength measurements were conducted using the same testbed shown in Fig. 1. However, for the breakdown measurements, the coupling capacitor and the PD measurement system were removed. For each sample, the voltage was slowly increased until the sinusoidal voltage collapsed to zero, which indicates a dielectric breakdown event. Subsequently, the breakdown voltage is divided by the thickness of each LMPC samples to derive the breakdown electric field E_{bd}.

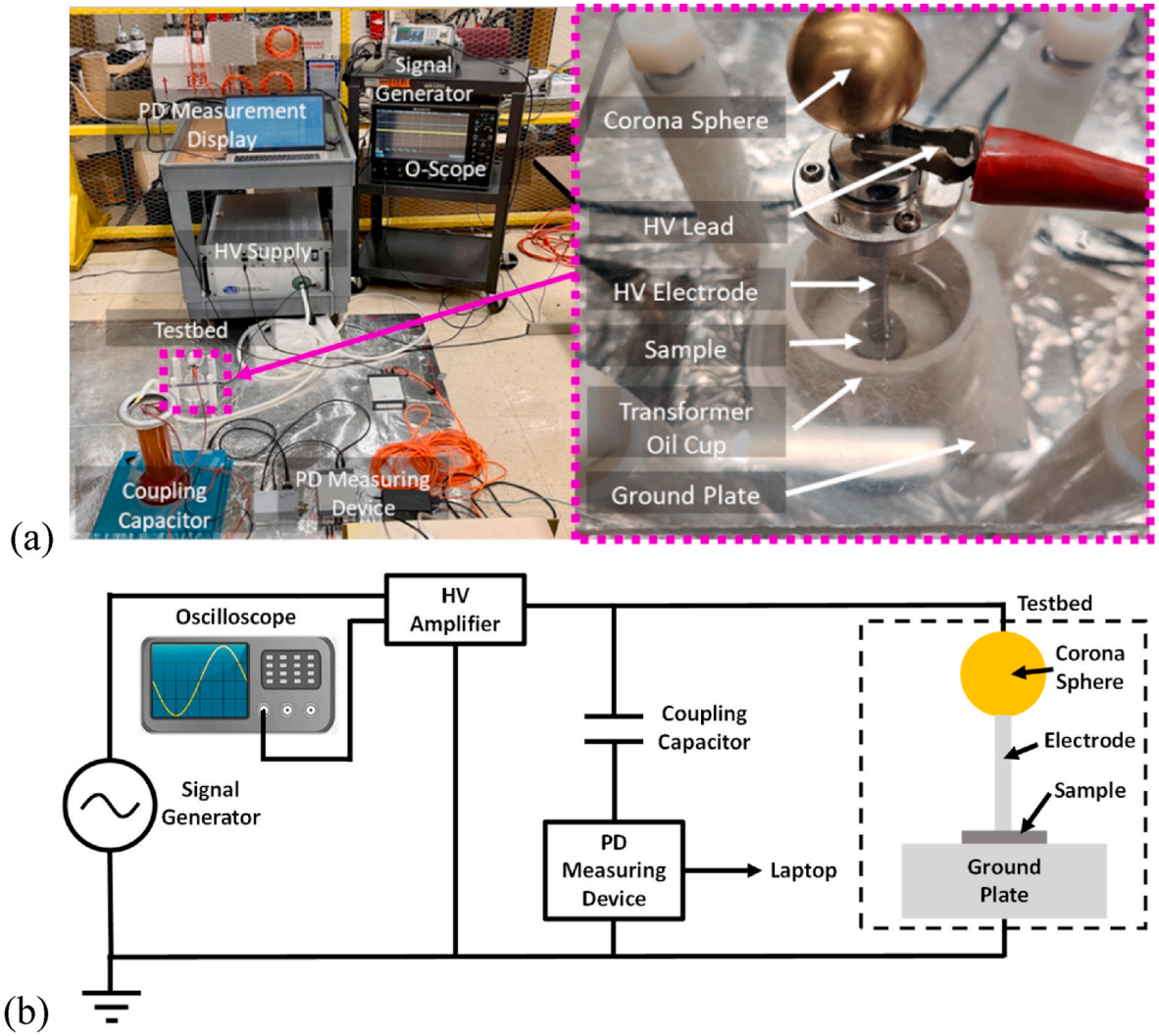

Fig. 1. Testbed used in this study. (a) Testbed for partial discharge (PD) and dielectric strength (E_{bd}) measurements, (b) circuit diagram of the testbed. (Note: the coupling capacitor and PD measurement device are not used for breakdown measurements.)

3. Experimental results

3.1. Dielectric loss (tan δ)

Dielectric loss (tan δ) indicates the amount of resistive current compared to capacitive current. It is measured by dividing resistive current by capacitive current. Dielectric materials with high tan δ lead to high leakage current and high Joule heating (i.e., power loss) while those with low tan δ result in low leakage current and low Joule heating. In general, low tan δ indicates high dielectric quality. The tan δ of the BTO composites was found to be largely frequency independent, while those of the GaInSn and Fe composites were frequency dependent. This relationship between the dielectric loss behavior and frequency has been observed previously for neat BTO composites [33] and neat Fe composites [34]. Dielectric loss was measured between the frequencies of 500 Hz to 5 MHz as shown in Figs. S1 and S2. Representative dielectric loss data shown in Figs. 2 and 3 were taken at 100.5 kHz, which was chosen due to the improved instrument sensitivity at this frequency. As shown in Figs. S1 and S2, the trends discussed here are true across frequencies, but a single frequency is discussed for clarity.

The tan δ of neat GaInSn, BTO, and Fe composites are shown in Fig. 2. For the neat GaInSn and BTO composites, increasing concentration has minimal impact on the dielectric loss. For the neat BTO composites, this is due to BTO having intrinsically low tan δ [35,36]. For the neat GaInSn composites, the tan δ may be largely unaffected by increasing concentration due to the oxide layer of the GaInSn droplets. The GaInSn oxide layer is primarily composed of gallium oxide which is known to lead to low losses in electrical applications [37,38]. The oxide of GaInSn likely results in shielding and mitigation of the lossy behavior (i.e., resistive current flow) of composite conductive material. Further demonstrating their low-loss performance, the tan δ values of the neat GaInSn and BTO composites are similar to that of PDMS (7.31×10^{-4} see Fig. S1). For the neat Fe composites, on the other hand, increasing Fe concentration increases tan δ due to an increase in conductive pathways formed by the Fe, allowing resistive current to flow more easily through these pathways. This results in the greater leakage current of the neat Fe composites leading to a decrease in the ability of the material to form an ideal capacitor.

The tan δ of the LMPCs and neat rigid filler composites were measured at varying concentrations of GaInSn, Fe, and BTO as shown in Fig. 3. As the amount of GaInSn is increased in the 10 and 20 vol% Fe containing LMPCs, the tan δ decreases, which may be due to the morphology of the composite (See Fig. S2). LMPCs of GaInSn and Fe show particle aggregation when observed through SEM imaging, specifically the GaInSn droplets "coat" the Fe particles (See Fig. S4). Due to this, the oxide layer of GaInSn droplets that coat the Fe particles are likely disrupting the Fe conductive pathways leading to a decrease in dielectric loss with increasing GaInSn concentration. However, upon

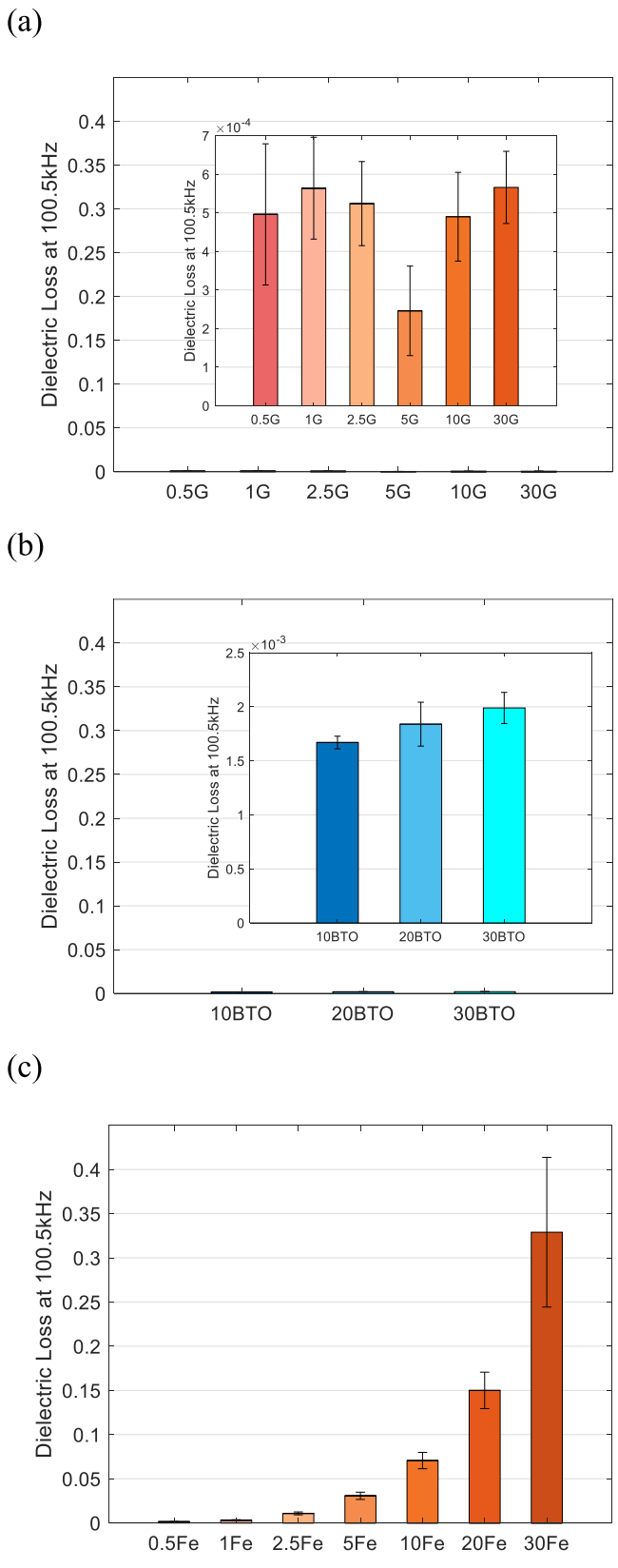

Fig. 2. Dielectric loss of neat dispersions of (a) GaInSn, (b) BTO, and (c) Fe at 100.5 kHz.

further increasing to 30 vol% Fe concentration, increasing the GaInSn concentration has little impact on the tan δ. This suggests that increasing Fe concentration results in less effective disruption of the Fe conductive pathways due to incomplete Fe particle coating. Alternatively, for the BTO containing LMPCs, increasing GaInSn concentration has little effect on the tan δ of the composites, which agrees with the observation that increasing GaInSn concentration on its own has little effect on tan δ, as seen in Fig. 2 (a). Comparatively, the tan δ of the BTO containing LMPCs is significantly smaller than that of the Fe containing LMPCs. This is due in part to Fe being a conductive material while BTO is an insulator which allows for less leakage of current, leading to a better performing dielectric material.

3.2. Partial discharge inception electric field (PDIE)

The PDIE of LMPCs was measured to identify the level of electric field that initiates the aging of the materials. BTO-GaInSn and Fe-GaInSn LMPCs were interrogated and reported in the following subsections.

3.2.1. PDIE of BTO-GaInSn composites

The PDIE measurements of BTO-GaInSn LMPCs are shown in Fig. 4. At a fixed concentration of 10 vol% BTO, PDIE drops steeply as the concentration of GaInSn increases. The composite containing 10 vol% GaInSn has a PDIE 74.6% lower than the neat BTO composite. As the GaInSn concentration is increased to 30 vol%, the PDIE further drops by 78.9%. At 20 vol% BTO, PDIE also decreases sharply as GaInSn concentration is increased with a 65.1% drop in PDIE between neat BTO and 10 vol% GaInSn and another 47.9% drop in PDIE as GaInSn concentration is increased to 30 vol%. A similar decreasing trend is observed in the 30 vol% BTO composites, where a drop in the PDIE of 66.3% occurs between neat BTO and 10 vol% GaInSn, and a drop in the PDIE of 63.6% occurs between 10 vol% GaInSn and 30 vol% GaInSn. Overall, it is observed that at any fixed concentration of BTO, increasing the concentration of GaInSn decreases PDIE. This is likely because GaInSn droplets in these composites have significantly large electrical conductivity and large average particle size compared to the BTO fillers. These factors cause larger areas of electric field enhancement within the LMPC sample leading to lower PDIE. Despite having a much higher conductivity and permittivity than PDMS, increasing BTO concentration has little effect on PDIE.

3.2.2. PDIE of PDMS-Fe-GaInSn composites

PDIE measurements in Fe-GaInSn LMPCs are shown in Fig. 5. These results indicate that PDIE decreases with increasing iron concentration. It should be noted that PDIE could not be measured for LMPCs containing more than 10 vol% iron as the sample broke down at a low enough voltage level such that our device could not accurately control nor measure PD. For 10 vol% iron, PDIE decreases with increasing GaInSn concentration from 0 vol% to 30 vol%. The decreasing trend is caused by increasing concentrations of GaInSn and Fe displacing the less conductive PDMS. Higher concentrations of Fe and GaInSn, which are both highly conductive, cause the electric field to become further concentrated in the remaining volume of PDMS. Also, the results show that Fe causes a much more dramatic decrease in PDIE than BTO. This is because the Fe particles not only have irregular shape with pointy edges, but also are larger in size than the BTO particles, causing larger areas of electric field enhancement like in the case of the GaInSn containing samples. The irregular, sharp, and jagged geometry of the Fe particles exacerbates this effect, with strong electric field enhancements occurring around the sharp edges.

3.3. Breakdown electric field (e_{bd})

The dielectric strength of the LMPCs was measured in terms of breakdown electric field (E_{bd}). BTO-GaInSn and Fe-GaInSn LMPCs were interrogated and reported in the following subsections.

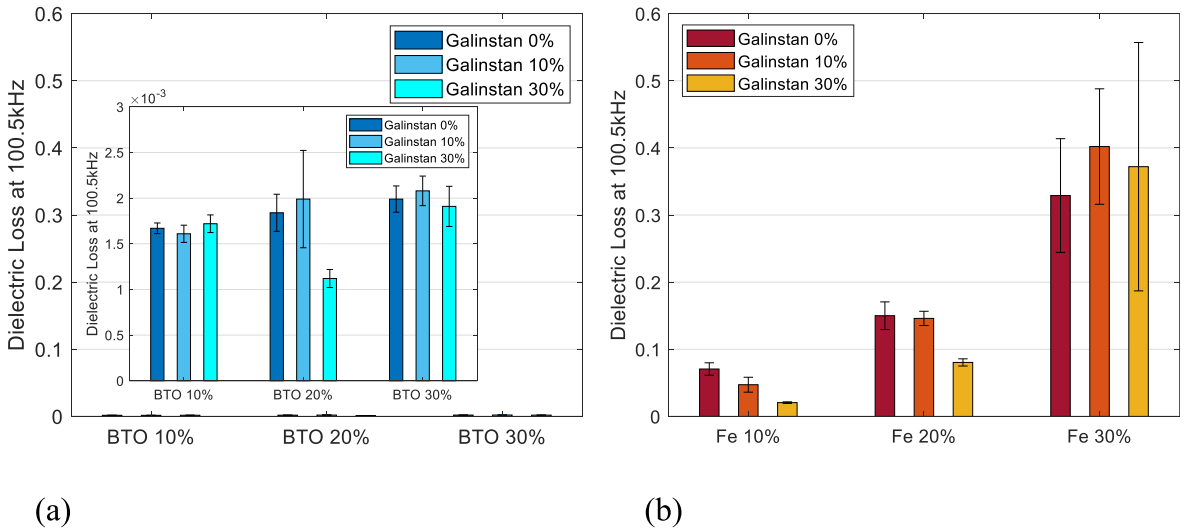

Fig. 3. Dielectric loss at 100.5 kHz for (a) BTO and (b) Fe dispersions of 10 vol%, 20 vol%, and 30 vol% with varying concentrations of GaInSn of 0 vol%, 10 vol%, and 30 vol%.

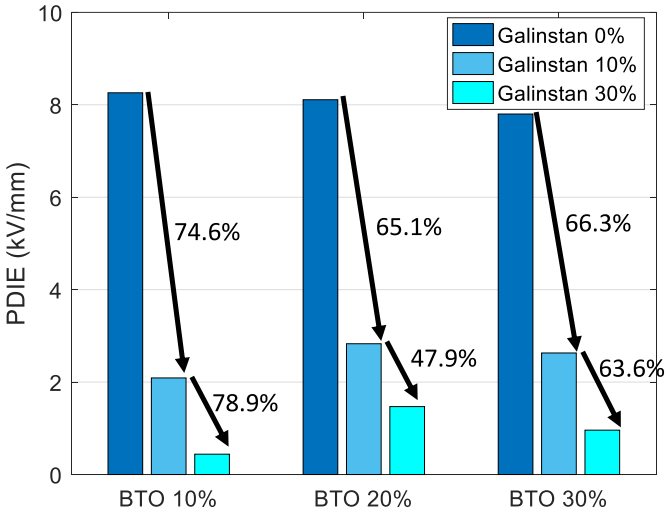

Fig. 4. PDIE of PDMS composed of BTO at 10 vol%, 20 vol%, and 30 vol% with varying concentrations of GaInSn of 0 vol%, 10 vol%, and 30 vol%.

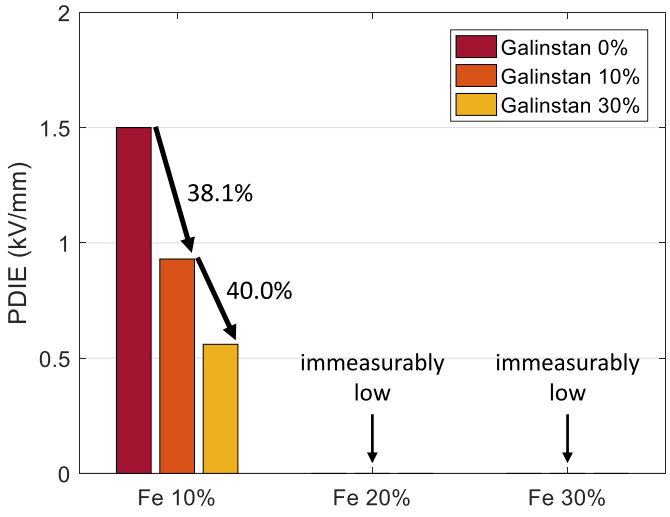

Fig. 5. PDIE of PDMS composed of Fe at 10 vol%, 20 vol%, and 30 vol% with varying concentrations of GaInSn of 0 vol%, 10 vol%, and 30 vol%.

3.3.1. E_{bd} of BTO-GaInSn composites

Dielectric breakdown measurements were conducted using the test-bed and equipment shown in Fig. 1. Fig. 6 details the E_{bd} measurements obtained from BTO-GaInSn composites. In composites containing 10 vol % BTO, a steep decreasing trend in E_{bd} is observed as the concentration of GaInSn is increased. The E_{bd} of the 10 vol%-10 vol% BTO-GaInSn composite is 73.2% lower than that of the neat 10 vol% BTO composite. As the concentration of GaInSn increases further to 30 vol%, the E_{bd} drops by an additional 73.9%. In the 20 vol% BTO composites, a 45% drop in E_{bd} occurs between neat BTO and 10 vol% GaInSn, and a 66.8% drop occurs between 10 vol% and 30 vol% GaInSn. At 30 vol% BTO, the E_{bd} of the 10 vol% GaInSn composite is 52.7% lower than that of the neat BTO composite, and the E_{bd} of the 30 vol% GaInSn composite is 57.2% lower than that of the 10 vol% GaInSn composite. At any fixed concentration of BTO, the E_{bd} decreases with increasing GaInSn concentration. This decreasing trend in E_{bd} with increasing GaInSn concentration is caused by the significantly high conductivity of GaInSn as compared to PDMS. The addition of fillers with a high conductivity or permittivity causes an increase in average electric field magnitude in the PDMS. This is mainly because the voltage drop is much smaller in the fillers with a high conductivity and permittivity compared to the substrate (i.e., PDMS), causing higher voltage drop (i.e., higher electric field) in the PDMS. As such, GaInSn has a more profound effect on E_{bd} than BTO primarily due to its much greater conductivity and larger particle size, which causes larger areas of electric field enhancement within the PDMS.

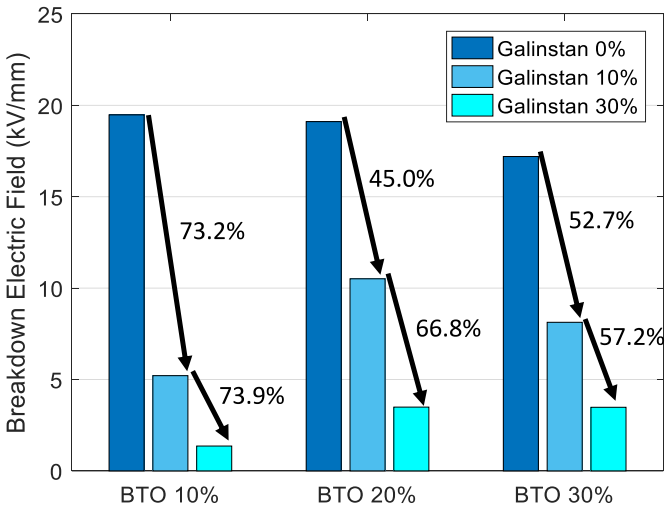

Fig. 6. Breakdown electric field of composites containing barium titanate of 10 vol%, 20 vol%, and 30 vol% with varying concentrations of galinstan of 0 vol%, 10 vol%, and 30 vol%.

3.3.2. E_{bd} of Fe-GaInSn composites

Fig. 7 shows the E_{bd} measurements of Fe-GaInSn composites. In composites containing 10 vol% Fe, the E_{bd} is 52.6% lower in the 10 vol% GaInSn composite than in the neat Fe composite, and the E_{bd} of the 30 vol% GaInSn composite is 33.9% lower than in the 10 vol% GaInSn composite. In composites containing 20 vol% Fe, the E_{bd} of the 10 vol% GaInSn composite is 73.1% lower than that of the neat Fe composite. However, the E_{bd} of the 30 vol% GaInSn composite is 37.7% higher than that of the 10 vol% GaInSn composite. This trend points to a more complex relationship between GaInSn and BTO, something that is evident throughout the electrical interrogation of these materials and is a focus for future work. In composites containing 30 vol% Fe, the E_{bd} decreased by 64.9% between neat Fe and 10 vol% GaInSn, and another 25.9% decrease occurred between 10 vol% GaInSn and 30 vol% GaInSn. At any fixed concentration of GaInSn, E_{bd} decreases as Fe concentration increases, and at any fixed Fe concentration, E_{bd} tends to decrease as GaInSn concentration increases. Overall, Fe containing LMPCs have a much lower E_{bd} than BTO containing LMPCs. The decreasing trend in E_{bd} and comparatively low E_{bd} in Fe containing LMPCs are caused by the high conductivity and permittivity of both GaInSn and Fe along with the irregular and sharp geometry of the Fe particles further increasing the local electric field. As both GaInSn and Fe have a much higher conductivity and permittivity than PDMS, the voltage drop occurs almost entirely in the PDMS. Also, higher filler concentration decreases the effective thickness of the PDMS, which leads to higher electric field in the PDMS. Furthermore, the sharp edges of the Fe particles cause local electric field enhancements, contributing to an increase in the average electric field in the PDMS.

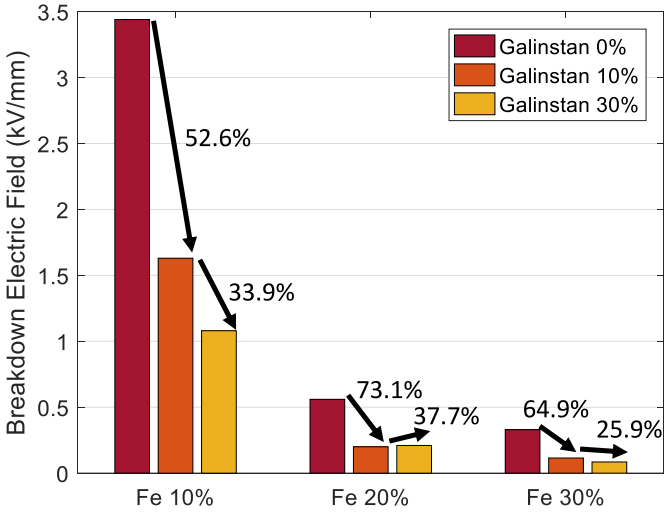

Fig. 7. E_{bd} of composites containing Fe of 10 vol%, 20 vol%, and 30 vol% with varying concentrations of GaInSn of 0 vol%, 10 vol%, and 30 vol%.

4. Discussion

The PDIE and E_{bd} of each LMPC are dependent on the overall filler concentration as well as the filler type. The filler properties that influence the dielectric properties of the LMPCs include conductivity, permittivity, filler particle size and shape. Fig. 8 shows the effects of filler type on E_{bd} and the simulated average electric field for single-filler LMPCs of 10 vol% and 30 vol% concentration. As shown in Fig. 8 (a), the neat BTO composite samples have the highest E_{bd} followed by neat GaInSn composites. Neat Fe composites show the lowest E_{bd} of any single filler composite. These differences in E_{bd} are caused by the combined effects of filler conductivity, permittivity, and geometry.

4.1. Effects of filler conductivity and permittivity

To determine the effects of conductivity and permittivity on the electric field distribution of a two-material composite while ignoring the effects of geometry, the LMPC composite is simplified to a two-layer stacked dielectric sandwiched between two thin conductors as shown in Fig. 9. The top conductor is energized to an arbitrary voltage v_{sys}, and the bottom conductor is connected to ground potential (i.e., 0 V). In this simplified model, the electric field in the second layer, which is assumed to have a lower conductivity and permittivity than the first layer, under steady state AC conditions is given by the formula $E_2 = (v_{sys} - E_1 d_1)/d_2$. As electric field is lower in materials with a higher conductivity or

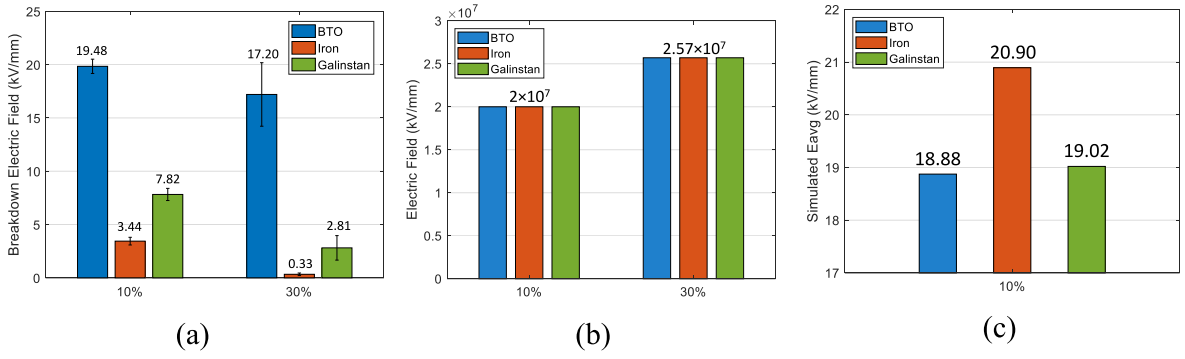

Fig. 8. Effects of filler type on (a) breakdown electric field measured via experiment, (b) electric field in PDMS calculated based on a simplified two-layer dielectric model shown in Fig. 9, and (c) average electric field derived from FEA models shown in Fig. 10.

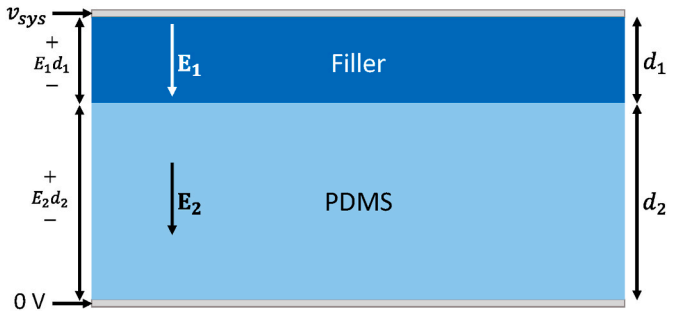

Fig. 9. Simplified two-layer dielectric model.

permittivity, the voltage drop $E_1 d_1$ is comparatively small. This causes a larger voltage drop and higher electric field (E_2) in the second layer that has a lower conductivity and permittivity. As filler concentration increases, the total thickness of PDMS (d_2) in the LMPC decreases, causing a stronger electric field in the PDMS (E_2).

4.2. Effects of filler geometry

In addition to studying the effects of conductivity and permittivity, an FEA environment is used to qualitatively explain the effects of filler geometry. In Fig. 10, a simplified 2D model with each sample represented by a rectangle is shown. The fillers are represented by circles for the BTO and GaInSn particles and ellipses for the Fe particles in an effort to emulate the true shape of the filler particles (see Figs. S5–S6 for SEM and digital microscopy images of the particles) while the spaces between the fillers in each sample are composed of PDMS. As the BTO used in the LMPCs tends to have a smaller particle size than GaInSn or Fe, the BTO particles were modeled at 0.1 times the cross-sectional area of the GaInSn and Fe particles. The conductivity and permittivity of each material used are shown in Table 1 [39,40]. The precise permittivity of the BTO filler is unknown as it depends on a variety of factors including the crystal structure and production method of the BTO [41]. For numerical electric field distribution analysis, a relative permittivity of 500 was assumed for BTO, which is a value reported in Ref. [39], while 1 was assumed for GaInSn and Fe. Fig. 10 shows the numerically analyzed electric field distribution of neat dispersions of BTO, GaInSn, and Fe at volume concentrations of 10% while an 18 kV, 60 Hz sinusoidal voltage stress is applied to the top edge of each sample. In the neat 10 vol% BTO LMPC, the simulated average electric field in the PDMS is 18.88 kV/mm. A higher average electric field of 19.02 kV/mm is observed in the 10 vol % GaInSn LMPC. The highest average electric field across the 10 vol% models occurred in the Fe LMPC at 20.90 kV/mm. A higher average electric field being formed at the same applied voltage coincides with a lower PDIE and lower breakdown electric field E_{bd}. This model provides insights into the experimental results by showing that PDMS-BTO composites have the lowest average electric fields, followed by PDMS-GaInSn and PDMS-Fe composites. These numerical results correspond to the fact that PDMS-BTO composites have the highest PDIE and E_{bd}, followed by PDMS-GaInSn and PDMS-Fe composites.

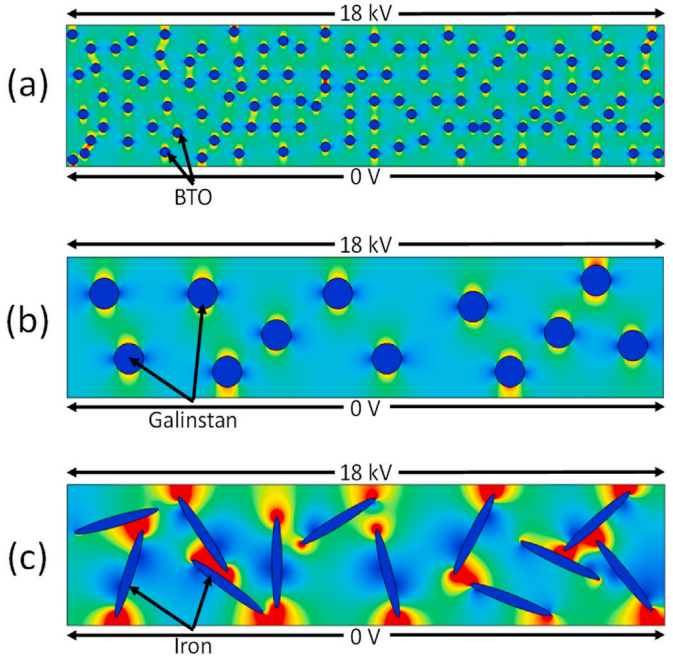

Fig. 10. Electric field distribution under 18 kV 60 Hz AC voltage stress. (a) 10% BTO, (b) 10% GaInSn, (c) 10% Fe.

Table 1
Material properties used in the FEA modeling shown in Fig. 10.

Material	Conductivity (S/m)	Relative Permittivity
PDMS	1×10^{-13}	2.86
GaInSn	3.46×10^{6}	1
Fe	1×10^{7}	1
BTO	2.5×10^{-6}	500

Results shown in Fig. 8 indicate that Fe increases tan δ and lowers PDIE and E_{bd} more significantly than any other fillers investigated due to the sharpness and irregular shape of the Fe particles. At a fixed voltage, the electric field magnitude surrounding a conductor is given by $E = V/r$. Sharp edges, which are expressed in terms of small r values, of the Fe particles cause a local electric field enhancement. Hence, a high concentration of sharp conductive particles in PDMS causes a significant increase in the average electric field, which explains the more pronounced effect of Fe on tan δ, PDIE, and E_{bd} compared to GaInSn. As an illustration of the effects of sharp edges, Fig. 11 shows a numerical model of a spherical GaInSn particle and an ellipsoidal Fe particle in a PDMS matrix with the top electrode energized at 18 kV. The electric field around the sharp edges of the Fe particle (ellipsoidal) is much greater in intensity than that around the GaInSn particle (spherical). The FEA simulation results suggest that the distinct geometry of Fe and GaInSn is one the reasons behind the substantially lower E_{bd} of the neat Fe LMPCs compared to that of the net GaInSn LMPCs. In general, an increase in the loading of a filler reduces E_{bd} because BTO, Fe, and GaInSn all have a much higher conductivity and permittivity than PDMS [40]. When relatively more conductive impurities or fillers are introduced into an electrically insulating medium, the electric field increase in magnitude in the bulk of the insulating medium and near the surface of the fillers due to their relatively small radii [42]. This means that a higher quantity of fillers increases the average electric field in the dielectric medium and, therefore, lowers the PDIE and E_{bd}.

According to the simplified model shown in Fig. 9, the calculated

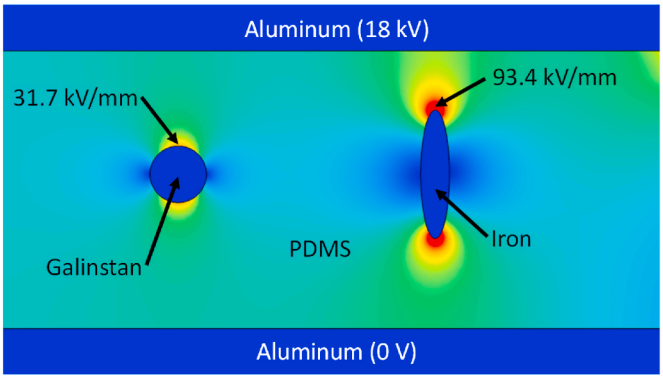

Fig. 11. The effects of filler geometry on electric field.

electric field in the PDMS, shown in Fig. 8 (b), electric field does not significantly depend on differences among the conductivity and permittivity of the fillers. This is because all of the three fillers studied have a conductivity many times higher than PDMS, causing differences in conductivity and permittivity between each filler to have a trivial effect on electric field distribution. This implies that the differences in particle size and shape are the primary contributors to the effects each of these fillers have on PDIE and E_{bd}. GaInSn and Fe each reduce PDIE and E_{bd} more dramatically than BTO because their larger particle size causing larger areas of electric field enhancement within the PDMS. Despite being slightly less than one order of magnitude more conductive than GaInSn, the Fe containing LMPCs broke down at a much lower electric field than the GaInSn LMPCs of the same concentration. This is most likely because while BTO and GaInSn particles are nearly spherical in shape, while Fe particles have an irregular shape with sharper edges (i.e., smaller radii). As discussed previously, it is well known that geometry has a profound effect on electric field due to Gauss's Law, where sharp edges cause local increases in electric field magnitude [42].

5. Conclusion

LMPC samples containing various concentrations of GaInSn along with a rigid filler, BTO or Fe of various concentrations, were fabricated and characterized. No clear trend in tan δ was found as GaInSn concentration increases, while increasing BTO and Fe concentration caused an increasing trend in tan δ. It was concluded that the PDIE of all samples tends to decrease with increasing BTO, GaInSn, or Fe concentration due to the higher conductivity and permittivity of these fillers compared to PDMS. In all composites, E_{bd} showed a trend similar to that of PDIE. Compared to other fillers, BTO tends to compromise dielectric integrity most weakly and Fe tends to compromise dielectric integrity most strongly by inducing the highest tan δ, lowest PDIE, and lowest E_{bd}. This conclusion was reinforced by FEA models that show strong spikes in electric field intensity near the sharp edges of the Fe particles along with a much higher average electric field in the bulk of the PDMS in neat Fe dispersions compared to the neat dispersions of GaInSn or BTO. The results suggest that incorporating BTO is a potential solution for fabricating LMPCs with improved dielectric reliability. With the results discussed in this work, it will be possible to strategically fabricate reliable and durable stretchable electronics and soft robotic devices with desired electrical properties by tuning filler composition and concentration.

Author statement

We declare that this manuscript is original, has not been published before and is not currently being considered for publication elsewhere. We confirm that the manuscript has been read and approved by all named authors and that there are no other persons who satisfied the criteria for authorship but are not listed. We further confirm that the order of authors listed in the manuscript has been approved by all of us.

Declaration of competing interest

We have no conflicts of interest to disclose.

Acknowledgements

This work has been sponsored by the National Science Foundation (NSF) through Award # 2124933 and 2124877.

Appendix A. Supplementary data

Supplementary data to this article can be found online at https://doi.org/10.1016/j.compositesb.2022.109686.

References

[1] Interfacial phenomena of advanced composite materials toward wearable platforms for biological and environmental monitoring sensors, armor, and soft robotics - horne - 2020 - advanced materials interfaces - Wiley Online Library." https://onlinelibrary.wiley.com/doi/abs/10.1002/admi.201901851 (accessed Nov. 01, 2021).
[2] Bury E, Chun S, Koh AS. Recent advances in deformable circuit components with liquid metal. Adv Electron Mater. 2021;7(4):2001006. https://doi.org/10.1002/aelm.202001006.
[3] Flexible electronics from intrinsically soft materials - ScienceDirect." https://www.sciencedirect.com/science/article/pii/S2666542521000072 (accessed Nov. 01, 2021).
[4] Wu W. Stretchable electronics: functional materials, fabrication strategies and applications. Sci Technol Adv Mater Dec. 2019;20(1):187–224. https://doi.org/10.1080/14686996.2018.1549460.
[5] Baptista R, Mendão A, Rodrigues F, Figueiredo-Pina CG, Guedes M, Marat-Mendes R. Effect of high graphite filler contents on the mechanical and tribological failure behavior of epoxy matrix composites. Theor Appl Fract Mech Oct. 2016;85:113–24. https://doi.org/10.1016/j.tafmec.2016.08.013.
[6] Park S, Park H, Seong S, Chung Y. Multilayer substrate to use brittle materials in flexible electronics. Sci Rep May 2020;10(1):7660. https://doi.org/10.1038/s41598-020-64057-6.
[7] T. Liu, P. Sen, and C.-J. Kim, "Characterization of nontoxic liquid-metal alloy galinstan for applications in microdevices," J Microelectromechanical Syst, vol. 21, no. 2, pp. 443–450, Apr. 2012, doi: 10.1109/JMEMS.2011.2174421.
[8] Markvicka EJ, Bartlett MD, Huang X, Majidi C. An autonomously electrically self-healing liquid metal–elastomer composite for robust soft-matter robotics and electronics. Nat Mater Jul. 2018;17(7):618–24. https://doi.org/10.1038/s41563-018-0084-7.
[9] Fassler A, Majidi C. Liquid-phase metal inclusions for a conductive polymer composite. Adv Mater 1928–1932;27(11). https://doi.org/10.1002/adma.201405256. Mar. 2015.
[10] M. D. Bartlett et al., "High thermal conductivity in soft elastomers with elongated liquid metal inclusions," Proc Natl Acad Sci U S Am, vol. 114, no. 9, pp. 2143–2148, Feb. 2017, doi: 10.1073/pnas.1616377114.
[11] Dickey MD. Stretchable and soft electronics using liquid metals. Adv. Mater. 2017;29(27):1606425. https://doi.org/10.1002/adma.201606425.
[12] Sensors | free full-text | soft and deformable sensors based on liquid metals | HTML." https://www.mdpi.com/1424-8220/19/19/4250/htm (accessed Nov. 01, 2021).
[13] Bo G, Ren L, Xu X, Du Y, Dou S. Recent progress on liquid metals and their applications. Adv Phys X Jan. 2018;3(1):1446359. https://doi.org/10.1080/23746149.2018.1446359.
[14] Pan C, et al. A liquid-metal–elastomer nanocomposite for stretchable dielectric materials. Adv Mater 2019;31(23):1900663. https://doi.org/10.1002/adma.201900663.
[15] Liquid metal–elastomer soft composites with independently controllable and highly tunable droplet size and volume loading | ACS applied materials & interfaces." https://pubs.acs.org/doi/full/10.1021/acsami.9b04569 (accessed Nov. 01, 2021).
[16] A. Koh, J. Sietins, G. Slipher, and R. Mrozek, "Deformable liquid metal polymer composites with tunable electronic and mechanical properties," J Mater Res, vol. 33, no. 17, pp. 2443–2453, Sep. 2018, doi: 10.1557/jmr.2018.209.
[17] Bartlett MD, Fassler A, Kazem N, Markvicka EJ, Mandal P, Majidi C. Stretchable, high-k dielectric elastomers through liquid-metal inclusions. Adv. Mater. 2016;28(19):3726–31. https://doi.org/10.1002/adma.201506243.
[18] Gao S, et al. Wearable high-dielectric-constant polymers with core–shell liquid metal inclusions for biomechanical energy harvesting and a self-powered user interface. J Mater Chem A 2019;7(12):7109–17. https://doi.org/10.1039/C9TA01249D.
[19] Cai L, Zhang S, Miao J, Yu Z, Wang C. Fully printed stretchable thin-film transistors and integrated logic circuits. ACS Nano Dec. 2016;10(12):11459–68. https://doi.org/10.1021/acsnano.6b07190.
[20] Yao S-H, Dang Z-M, Jiang M-J, Bai J. BaTiO3-carbon nanotube/polyvinylidene fluoride three-phase composites with high dielectric constant and low dielectric loss. Appl Phys Lett Nov. 2008;93(18). https://doi.org/10.1063/1.3013833. 182905.
[21] Saini P, Arora M, Gupta G, Gupta B, Singh VN, Choudhary V. High permittivity polyaniline–barium titanate nanocomposites with excellent electromagnetic interference shielding response. Nanoscale 2013;5(Apr). https://doi.org/10.1039/c3nr00634d.
[22] Carpi F, Migliore A, Serra G, Rossi DD. Helical dielectric elastomer actuators. Smart Mater Struct Dec. 2005;14(6):1210–6. https://doi.org/10.1088/0964-1726/14/6/014.
[23] Merhebi S, et al. Magnetic and conductive liquid metal gels. ACS Appl Mater Interfaces Apr. 2020;12(17). https://doi.org/10.1021/acsami.0c03166. 20119–20128.
[24] Cao L, et al. Ferromagnetic liquid metal putty-like material with transformed shape and reconfigurable polarity. Adv. Mater. 2020;32(17):2000827. https://doi.org/10.1002/adma.202000827.
[25] L. Hu, H. Wang, X. Wang, X. Liu, J. Guo, and J. Liu, "Magnetic liquid metals manipulated in the three-dimensional free space," ACS Appl Mater Interfaces, vol. 11, no. 8, pp. 8685–8692, Feb. 2019, doi: 10.1021/acsami.8b22699.

[26] Yun G, et al. Liquid metal-filled magnetorheological elastomer with positive piezoconductivity. Nat Commun 2019;10(1):1300. https://doi.org/10.1038/s41467-019-09325-4. Mar.
[27] Guo R, Sun X, Yuan B, Wang H, Liu J. Magnetic liquid metal (Fe-EGaIn) based multifunctional electronics for remote self-healing materials, degradable electronics, and thermal transfer printing. Adv Sci 2019;6(20):1901478. https://doi.org/10.1002/advs.201901478.
[28] A general approach to composites containing nonmetallic fillers and liquid gallium." https://www.science.org/doi/10.1126/sciadv.abe3767 (accessed Nov. 01, 2021).
[29] Yun G, et al. Liquid metal hybrid composites with high-sensitivity and large dynamic range enabled by micro- and macrostructure engineering. ACS Appl. Polym. Mater. Oct. 2021;3(10):5302–15. https://doi.org/10.1021/acsapm.1c01111.
[30] S.-Y. Fu, X.-Q. Feng, B. Lauke, and Y.-W. Mai, "Effects of particle size, particle/matrix interface adhesion and particle loading on mechanical properties of particulate–polymer composites," Compos B Eng, vol. 39, no. 6, pp. 933–961, Sep. 2008, doi: 10.1016/j.compositesb.2008.01.002.
[31] Powell RW. Further measurements of the thermal and electrical conductivity of iron at high temperatures. Proc Phys Soc May 1939;51(3):407–18. https://doi.org/10.1088/0959-5309/51/3/304.
[32] J. Gao et al., "Designing high dielectric permittivity material in barium titanate," J Phys Chem C, vol. 121, no. 24, pp. 13106–13113, Jun. 2017, doi: 10.1021/acs.jpcc.7b04636.
[33] M. Matsumoto and Y. Miyata, "Complex permittivity based on equivalent circuit model for polymer/metal composite. Frequency dependence of permittivity as function of concentration," IEEE Trans Dielectr Electr Insul, vol. 6, no. 1, pp. 27–34, Feb. 1999, doi: 10.1109/94.752006.
[34] S. Siddabattuni, T. P. Schuman, and F. Dogan, "Improved polymer nanocomposite dielectric breakdown performance through barium titanate to epoxy interface control," Mater Sci Eng B, vol. 176, no. 18, pp. 1422–1429, Nov. 2011, doi: 10.1016/j.mseb.2011.07.025.
[35] Vijatović MM, Bobić JD, Stojanović BD. History and challenges of barium titanate: Part II. Sci Sinter 2008;40(3):235–44.
[36] M. N. Almadhoun et al., "Bipolar resistive switching in junctions of gallium oxide and p-type silicon," Nano Lett, vol. 21, no. 6, pp. 2666–2674, Mar. 2021, doi: 10.1021/acs.nanolett.1c00539.
[37] Roy S, et al. Correlation between structure, chemistry, and dielectric properties of iron-doped gallium oxide (Ga2–xFexO3). J Phys Chem C Dec. 2018;122(48):27597–607. https://doi.org/10.1021/acs.jpcc.8b07921.
[38] Dang Z-M, Zha J-W, Yu Y, Zhou T, Song H-T, Li S-T. Microstructure and dielectric characterization of micro- nanosize co-filled composite films with high dielectric permittivity. IEEE Trans Dielectr Electr Insul Oct. 2011;18(5):1518–25. https://doi.org/10.1109/TDEI.2011.6032820.
[39] Yustanti E, Hafizah MAE, Manaf A. Enhanced dielectric properties of Nanocrystalline Ba(1-x)SrxTiO3 (x=0 and 0.3) ceramics. IOP Conf Ser: Earth Environ Sci Jan. 2018;105:12072. https://doi.org/10.1088/1755-1315/105/1/012072.
[40] Park C. Electret: an entirely new approach of solving partial discharge caused by triple points, sharp edges, bubbles, and airgaps. IEEE Access 2020;8:78354–66. https://doi.org/10.1109/ACCESS.2020.2990310.
[41] Osman KI. SYNTHESIS AND CHARACTERIZATION OF BaTiO3 FERROELECTRIC MATERIAL, vol. 176; 2011.
[42] Küchler A. In: Küchler A, editor. "Electric stresses," in *high voltage engineering: fundamentals - technology - applications*. Berlin, Heidelberg: Springer; 2018. p. 5–140. https://doi.org/10.1007/978-3-642-11993-4_2.